Characterization of the electrical contact between a conductive atomic force microscope cantilever and a carbon nanotube

Tarek K. Ghanem, Ellen D. Williams, and Michael S. Fuhrer[a)]
Department of Physics and Center for Nanophysics and Advanced Materials, University of Maryland, College Park, Maryland 20742-4111, USA

(Received 11 April 2011; accepted 21 July 2011; published online 1 September 2011)

A full characterization of the electrical contact between conductive atomic force microscope (AFM) cantilevers and carbon nanotubes (CNTs) is presented. The dependence of current through the contact on loading force, geometric parameters, bias conditions, and time is studied in a two-terminal configuration, where a gold coated AFM cantilever serves as a movable electrode. We find that for an optimized placement of the cantilever relative to the CNT, the current through the contact becomes independent of the loading force beyond a certain limit, and this behavior is also independent of bias conditions. In that load-independent regime, the contact is stable in time to within the current fluctuations imposed by $1/f$ and telegraph noise in the CNT channel. Under certain conditions of tip placement, the current through the contact exhibits a non-monotonic behavior with loading, which is well explained by the parasitic planar motion of the cantilever.
© *2011 American Institute of Physics*. [doi:10.1063/1.3626811]

I. INTRODUCTION

Employing a conductive AFM cantilever as a movable electrode to perform electrical transport measurements in carbon nanotubes (CNTs) is a technique that has been frequently reported in literature.[1–6] The main reason for using this technique is to measure transport properties as a function of channel length, thus separating contact effects[3,7] from the intrinsic response of the CNT channel, which is important for understanding scattering mechanisms,[4,7] and possibly other transport phenomena such as localization.[2,6] Despite the large volume of work using this technique, only a few attempts at characterization have been made,[1,8,9] where the obtained responses were analyzed in terms of band structure modulation caused by the radial deformation of the CNT,[10–14] which is induced by the tip at the contact point.

For the movable electrode technique, the contact resistance between the CNT and the metal coated AFM cantilever will change every time the contact is established, which causes an undesirable scatter in length-dependent transport data. This problem can usually be circumnavigated by using a three-terminal technique.[3,4] However, it is still important to understand how to obtain these temporary contacts in a controlled and reproducible manner, and the variables which affect them.

In the current work, a full characterization of the electrical contact between conductive AFM cantilevers and CNTs is presented. We employ a two-terminal configuration, as is shown in Fig. 1, where the CNT channel is defined between a fixed electrode and a point that is contacted by the conductive AFM cantilever. The conductive cantilever also provides the drain voltage, V_d, while the backgate provides the gate voltage, V_g. Measurements were performed on seven different CNTs whose properties are summarized in Table I. Our measurements indicate that an important factor is the parasitic planar motion acquired by the AFM tip during loading, which can cause diverse current versus loading behavior. The measurements also indicate that a properly positioned cantilever forms a stable reproducible contact with the CNT where the contact resistance is independent of the loading force beyond a certain limit, and that this behavior is largely independent of the bias conditions.

[a)]Author to whom correspondence should be addressed. Electronic mail: mfuhrer@physics.umd.edu.

II. EXPERIMENTAL SETUP

We used chemical vapor deposition (CVD) to grow CNTs according to published recipes.[15,16] The substrate used is heavily doped Si which has a 500 nm oxide layer and also serves as a backgate. After CVD, we thermally evaporated a single gold electrode (without an adhesion layer) which is defined by a shadow mask. Gold has been reported before to form ohmic contacts to CNTs.[2,3] After the gold evaporation, the sample is fixed to a suitable holder, wire bonded, and installed in an AFM (model Dimension 5000 from Veeco Instruments) which is also equipped with a closed loop

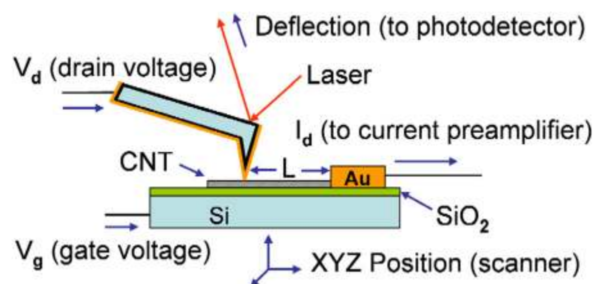

FIG. 1. (Color online) Schematic of the measurement system. The CNT channel is defined between the fixed gold electrode and the gold-coated AFM cantilever. The X- and Y-positions of the scanner determine the channel length L, and the Z-position determines the deflection (contact force) between the surface and the tip. V_d and V_g determine the current, I_d, through the channel.

 © 2011 American Institute of Physics

Downloaded 01 Sep 2011 to 129.2.99.26. Redistribution subject to AIP license or copyright; see http://jap.aip.org/about/rights_and_permissions

TABLE I. Designation, type (semiconducting or metallic), and diameter d of the CNTs studied.

CNT	Type	d (nm)
D1	semiconducting	2.1
D2	metallic	2.2
D3	semiconducting	3.0
D4	metallic	4.1
D5	semiconducting	1.9
D6	metallic	4.0
D7	metallic	2.0

scanner (model NPXYZ100B from nPoint, Inc.). We used two different types of AFM cantilevers in our measurements, FESP ($k = 2.8$ N/m) and LTESP ($k = 48$ N/m), both from Veeco Instruments. We will refer to these as 'soft cantilevers,' and 'hard cantilevers,' respectively. To make them conductive, we coated the raw Si cantilevers with a 50–60 nm layer of titanium followed by 60–90 nm of gold using thermal evaporation. The outer gold coating is what contacts the CNTs.

The measurement procedure begins by searching, via conventional intermittent-contact AFM imaging, for a CNT that is contacted by the fixed gold electrode at one end. Then the AFM scanning motion and the AC vibrations of the cantilever are stopped. The cantilever is positioned and brought down to the surface such that it contacts the CNT somewhere between its free end and the fixed electrode.

The formation of a cantilever-CNT contact can be expected to have both electronic and mechanical aspects, and therefore, it depends on the parameters of both the CNT and the cantilever. The parameters related to the metal coated AFM cantilever are its force constant, its dimensions, and the coating metal, which, in the case of semiconducting CNTs, determines whether the electrical contact is of the Ohmic or Schottky barrier type.[17,18] The relevant parameters for the CNT are its type, i.e., whether it is metallic or semiconducting, its diameter (which determines the bandgap for a semiconducting CNT), and its geometric orientation relative to the cantilever. We also studied the dependence of the contact on the lateral position (i.e., the position along the direction normal to the CNT axis) of the tip relative to the CNT. We will discuss the dependence of the contact on these parameters in the next sections.

III. RESULTS AND DISCUSSION

A. Conductance versus load behavior

To investigate the behavior of the contact as a function of loading force, points along the CNTs were selected as described in Sec. II. At each of these positions, we performed a number of loading cycles where the cantilever is lowered in successive steps of $\delta Z = 2.5$ nm, and we simultaneously recorded the Z-displacement of the scanner, deflection of the cantilever, and current passing through the CNT device after each step, until a specified deflection setpoint was reached. Then the same procedure was repeated with the cantilever moving up, until the mechanical contact with the surface was lost. We will refer to these measurements throughout as "current-loading curves," where "loading" here means either loading or unloading.

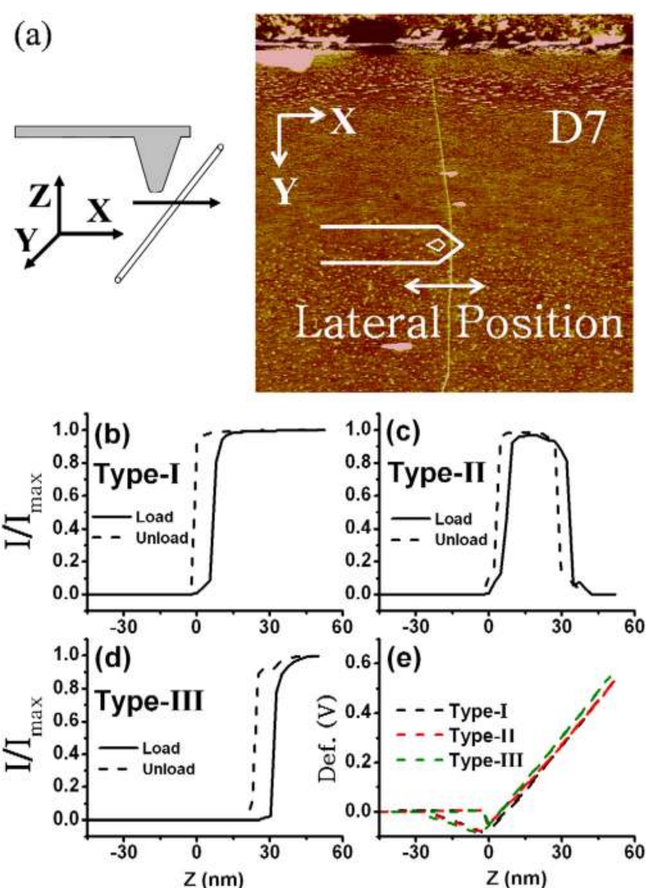

FIG. 2. (Color online) (a) Illustration of the "perpendicular profile" measurement geometry, scan size is 10×10 μm (cantilever is not drawn to scale). The edge of the fixed gold electrode can be seen on top. (b)-(d) Current-loading curves of Types-I, II, and III, respectively, $Z = 0$ is defined at the onset of mechanical contact. (e) Deflection corresponding to the three loading cycles, used to define $Z = 0$. Data in (b) through (d) are taken at the same point on CNT D7, 19.0 μm away from the fixed gold electrode with different lateral positions about 25 nm apart (along the X-axis), $V_d = 0.1$ V, $V_g = -3.0$ V, and $I_{max} = 0.21$ μA. The cantilever used is a soft cantilever.

At each point along the CNT, we changed the lateral position (perpendicular to the CNT axis) of the cantilever by a few nanometers, and repeated the measurement at each lateral position. The purpose was to investigate whether there is an optimal combination of loading force and lateral position that would minimize the contact resistance between the cantilever and the CNT. One extreme of the measurement geometry is when the CNT orientation is perpendicular to the long axis of the cantilever, and therefore the lateral position is adjusted in the X-direction, as shown in Fig. 2(a). We will henceforth term this geometry a "perpendicular profile." In this geometry, we observed three distinct types of behavior for current-loading curves. These types are shown in Figs. 2(b) through 2(d). The cantilever deflection for these loading cycles is also shown in Fig. 2(e).

For current-loading curves of Type-I represented by Fig. 2(b), conduction through the CNT device starts simultaneously with the mechanical contact (which we define as $Z = 0$), and the current rises quickly with more loading,

Downloaded 01 Sep 2011 to 129.2.99.26. Redistribution subject to AIP license or copyright; see http://jap.aip.org/about/rights_and_permissions

finally reaching a load-independent value. In current-loading curves of Type-II, represented by Fig. 2(c), the contact starts similar to Type-I, but the current rises and then goes back to zero with more loading, and the current may or may not reach its maximum possible value in the middle. In current-loading curves of Type-III, represented by Fig. 2(d), electrical conduction is delayed beyond the mechanical contact, and then starts to behave similarly to Type-I with more loading. Unloading generally shows similar behavior to loading, with hysteresis caused by adhesion. Responses which are somewhat similar to current-loading curves of Type-I and Type-II have been reported before in the literature.[1,8,9] We have observed these three types of behavior for all of the CNTs we studied, whether metallic or semiconducting. This behavior was largely independent of the cantilever force constant and contact type (we obtained Schottky barrier contacts using a tip covered only with Ti). The behavior observed exclusively depended on the lateral position of the cantilever relative to the CNT.

In order to systematically study the occurrence of these types of current-loading curves, we uniformly collected current-loading curves as a function of the lateral position (X-position in this case). We started at a lateral position far off the desired location on the CNT, and then we moved the cantilever toward the CNT, changing the lateral position by uniform increments of 2–6 nm, performing a single loading cycle at every point, and going across the CNT until contact is achieved and then lost again. The current-loading curves obtained at the various lateral positions are stacked together in a matrix form, which is represented as a 2-D contour map of the current passing through the device as a function of the lateral position and Z-displacement of the scanner. Examples of these are shown in Fig. 3 for points on CNTs D2 and D3. Notice that current-loading curves are vertical slices through these 2-D maps.

The main features observed in these perpendicular profiles are: (1) the occurrence of the different types of current-loading curves follows a specific sequence; starting from low lateral displacement values, we initially get curves of Type-III, followed by Type-I and then Type-II, respectively; (2) the maps consist of fast rising edges that surround a wide plateau, where the current through the contact is largely independent of the loading force; (3) this behavior is independent of the type of the CNT, since these profiles look the same for D3 which is semiconducting, and D2 which is metallic; (4) the left and right edges of the plateaus (which correspond to Type-III and Type-II current-loading curves, respectively) are linear and have almost the same slopes, which possibly indicates a common origin for both types of behavior, and this linear relation at the profile edges can be written as,

$$\Delta X = \beta \Delta Z, \tag{1}$$

where β is the inverse slope. The experimentally found values of $\beta \approx 0.26$–0.30 were generally independent of the type of the CNT or any other parameter, and were also similar for both types of cantilevers used.

In order to study the orientation dependence of these profiles, we used CNTs D4 and D6 because they had naturally formed loops, as shown in Fig. 4(a) for the case of D6, and therefore they had portions where the CNT is parallel to the long axis of the cantilever. This represents the other extreme of the measurement geometry where the lateral position is now changed in the Y-direction rather than the X-direction. We shall term this geometry a "parallel profile." Figure 4(b) shows one such profile, which can be seen to have a significantly different boundary shape from the perpendicular profiles shown previously in Fig. 3, with the beginning and the end of the plateau having almost vertical edges. In other words, a parallel profile consists only of Type-I current-loading curves. It is worth mentioning here that perpendicular profiles taken on other suitable portions of the same CNTs had the same characteristics of perpendicular profiles previously mentioned, which indicates that the difference between perpendicular and parallel profiles is only caused by the CNT orientation relative to the cantilever.

These observations can be well explained by noticing that the cantilever does not apply force to the surface like a solid piston. Upon loading, the AFM tip acquires a parasitic planar motion and slides on the surface.[19–21] This

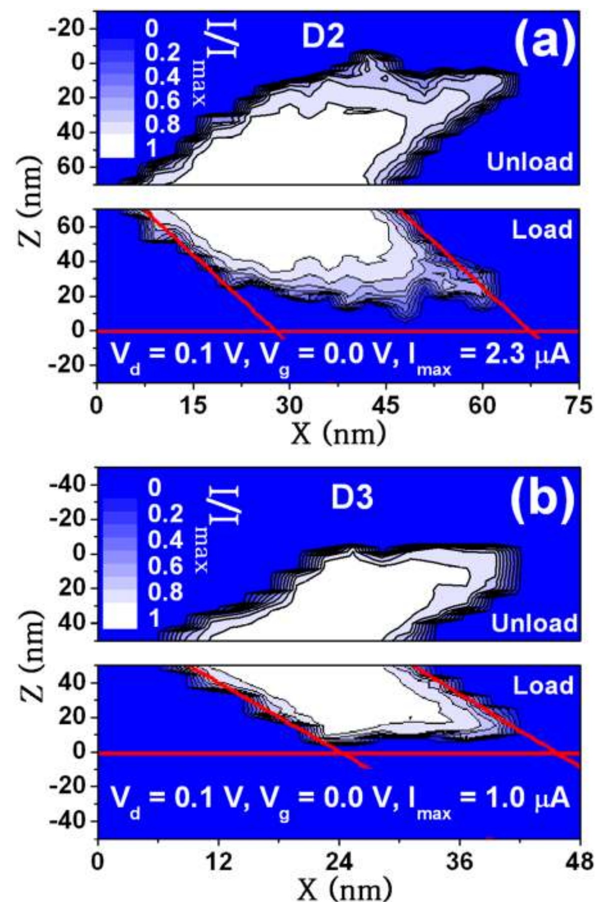

FIG. 3. (Color online) (a) Two-dimensional plots of current vs both lateral position X and loading Z taken in the "perpendicular profile" configuration of Fig. 2(a) on the metallic CNT D2, 5.9 μm away from the fixed electrode, with $V_d = 0.1$ V, $V_g = 0.0$ V, and $I_{max} = 2.3$ μA. (b) Same as (a) for the semiconducting CNT D3, 6.6 μm away from the fixed electrode, with $V_d = 0.1$ V, $V_g = 0.0$ V, and $I_{max} = 1.0$ μA. The horizontal red lines indicate the onset of mechanical contact at Z = 0 and the sloped red lines indicate the profiles' boundaries. These have a slope of 3.4 in both (a) and (b) corresponding to an inverse slope of 0.29. Both maps are obtained using soft cantilevers.

Downloaded 01 Sep 2011 to 129.2.99.26. Redistribution subject to AIP license or copyright; see http://jap.aip.org/about/rights_and_permissions

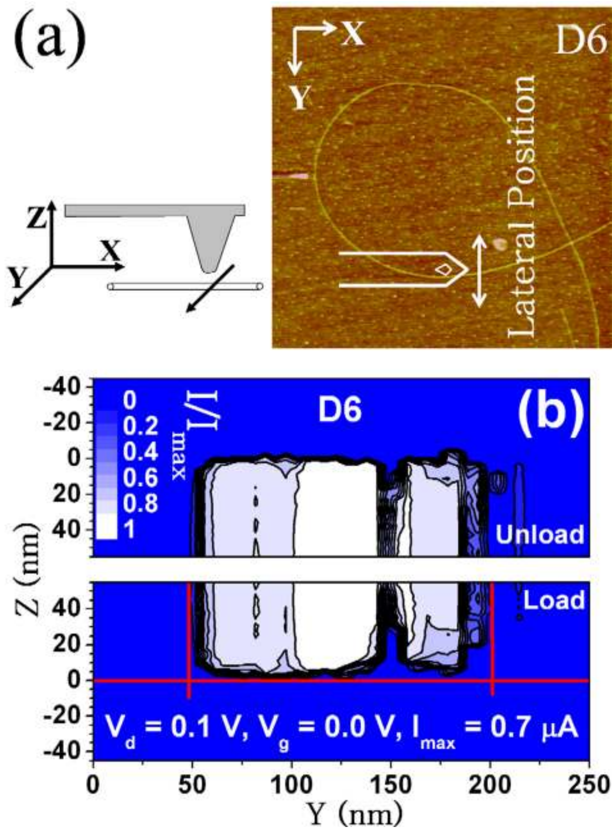

FIG. 4. (Color online) (a) Illustration of the "parallel profile" measurement geometry, scan size is 10×10 μm (cantilever not drawn to scale). (b) Two-dimensional plot of current vs both lateral position Y and loading Z taken in the parallel profile configuration shown in (a), the vertical boundaries indicate the presence of only Type-I current-loading curves. The point where the profile was taken is illustrated in (a), 4.8 μm from the loop junction, which is 17.8 μm away from the fixed electrode. $V_d = 0.1$ V, $V_g = 0.0$ V, and $I_{max} = 0.7$ μA. The map is obtained using a hard cantilever.

mechanical motion can explain the observed behaviors through the tip sliding away, or toward, the CNT. Following Huang *et al.*,[20] the relation between the Z-displacement of the cantilever and the parasitic planar displacement (this displacement is along the long axis of the cantilever, which is always the X-direction in our setup) is provided by,

$$\Delta X = (\tan\theta + 3h_t/2L_c)\Delta Z, \tag{2}$$

where θ is the cantilever mounting angle, h_t is the height of the tip, and L_c is the length of the cantilever. In our setup $\theta = 12°$, and both types of cantilevers used have the typical values $L_c = 225$ μm and $h_t = 12$ μm. Using these values, the term between the brackets in Eq. (2) which represents the inverse slope β in Eq. (1) can be found to be 0.29, which is in good agreement with the experimentally found values of $\beta \approx 0.26$–0.3 for both types of cantilevers.

Now the current versus loading behavior of both profile types can be qualitatively explained. In the perpendicular profile configuration, Type-III current-loading curves are produced by the tip landing too far from the CNT, and as loading increases, it slides and contacts the CNT. Type-II can be explained as the tip initially landing on the CNT and as loading increases, the tip slides off the CNT and electrical contact is lost. Finally for Type-I, the tip initially lands on the CNT, however the parasitic planar motion corresponding to the designated deflection setpoint is not enough to break the contact before the deflection setpoint is reached. For the parallel profile geometry, the cantilever slides along the axis of the CNT, therefore the contact is never lost with more loading and Type-I behavior is always obtained. These situations are schematically shown in Fig. 5.

It must be emphasized here that all the diverse switching behavior reported above is of a purely mechanical origin, and this should be taken into account before invoking any interpretation of current versus loading behavior in terms of material properties at the contact. This also might offer a simpler explanation for some of the non-monotonic current-loading behaviors reported in the literature for CNTs.[8,9]

B. Dependence on bias conditions

We have observed Type-I current-loading curves in all of the loading experiments we performed on both metallic and semiconducting CNTs, and we conclude that they are always obtainable with the proper adjustment of the lateral position of the cantilever. Furthermore, the current through the CNTs in the load-independent regime was highly reproducible upon breaking and remaking of the contact several times, indicating no permanent change of the CNT at the contact point. We therefore assume that Type-I current-loading curves approximate the true loading behavior of the contact. This is extremely useful when performing local transport measurements because it means that finding the minimum contact resistance, $(R_c)_{\min}$, is only a matter of using the correct deflection setpoint such that the current is in the load-independent regime, and finding the optimal lateral position where the maximum current is achieved. Now the local transport problem of measuring $R(V_d,V_g,L,R_c)$, where R_c varies randomly with L, can be effectively reduced

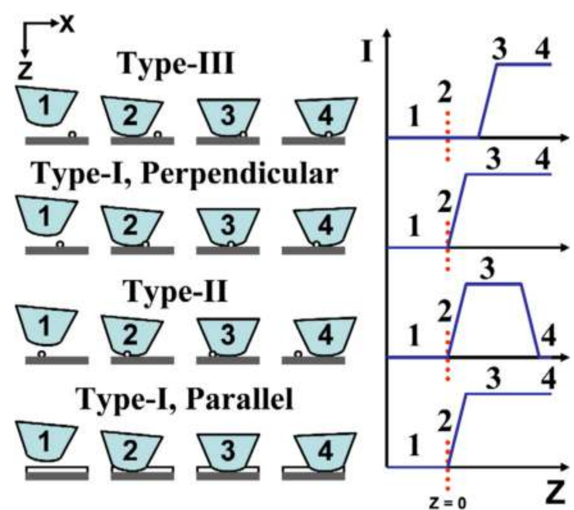

FIG. 5. (Color online) Explanation of current-loading curves. (1) Cantilever approaching the surface, no current flow. (2) Cantilever snaps into mechanical contact with the surface, with onset of current flow, except for Type-III where the cantilever lands far to the left. (3) Cantilever slides on the surface with loading, still maintaining contact with the CNT, or initiating contact for the case of Type-III. (4) The cantilever keeps on sliding with more loading and contact is maintained, except for Type-II where the cantilever initially landed far to the right.

Downloaded 01 Sep 2011 to 129.2.99.26. Redistribution subject to AIP license or copyright; see http://jap.aip.org/about/rights_and_permissions

into $R(V_d,V_g,L)$, with R_c now being a constant equal to $(R_c)_{\min}$.

We have also verified that Type-I behavior is independent of the bias conditions, V_d and V_g. In order to check that, we first adjust the lateral position such that Type-I current-loading curves are obtained, then we start a loading cycle where, instead of measuring a single current point at constant bias conditions for each increment of the Z-displacement, we sweep either V_d or V_g while keeping the other voltage constant.

Figure 6 shows the results, presented in the form of 2-D contour maps of constant current as a function of Z-displacement and either V_d or V_g, for both semiconducting and metallic CNTs. We can observe that briefly after the contact is established, the constant current contours take the shape of straight horizontal lines, thus confirming the robustness of Type-I behavior against variations in either V_d or V_g, in both semiconducting and metallic CNTs.

C. Electromechanics at the contact

The resistance of a CNT under loading by a conductive AFM cantilever can be written as $R(\mathrm{Z}) = R_{nt}(L) + R_{Au} + R_c(\mathrm{Z})$, where $R_{nt}(L)$ is the length-dependent CNT channel resistance, R_{Au} is the contact resistance at the fixed gold electrode, and $R_c(\mathrm{Z})$ is the load-dependent contact resistance, respectively. We further assume that $R_c(\mathrm{Z}) = (R_c)_{\min} + \Delta R_c(\mathrm{Z})$. From measuring the resistance at very short channel lengths, < 0.5 μm, we deduce that $R_{Au} + (R_c)_{\min}$ is typically 10-18 kΩ, close to the theoretical minimum, $h/4e^2 = 6.5$ kΩ. The gate modulation of these resistances was rather mild, typically causing them to rise within $10 \pm 3\%$ as V_g is swept from -10 to $+10$ V.

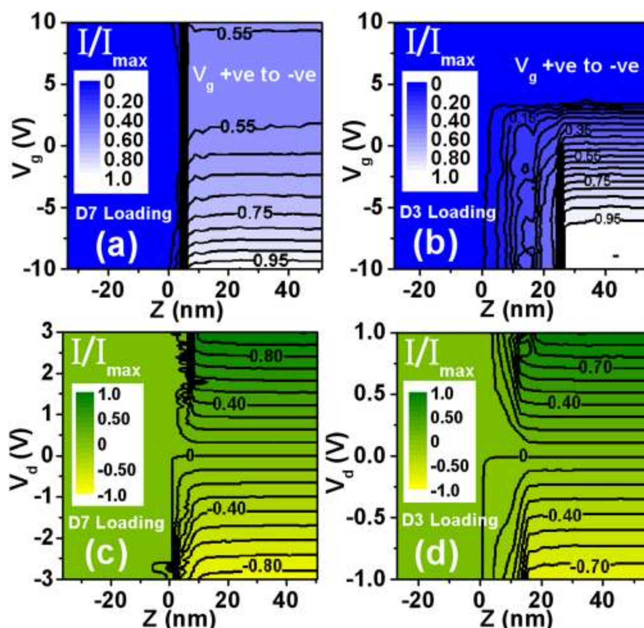

FIG. 6. (Color online) (a) Constant drain current contours as a function of both V_g and loading Z for metallic CNT D7. $I_{\max} = 2.8$ μA, and $V_d = 0.1$ V. (b) Same as (a) for semiconducting CNT D3 with $I_{\max} = 1.1$ μA, and $V_d = 0.1$ V. (c) Constant drain current contours as a function of both V_d and loading Z for CNT D7. $I_{\max} = 5.5$ μA, and $V_g = 0.0$ V. (d) Same as (c) for CNT D3 with $I_{\max} = 0.74$ μA, and $V_g = -2.5$ V. The maps in (a) and (c) are recorded 19.1 μm away from the fixed electrode, and (b) and (d) are recorded 87 μm away from the fixed electrode. The onset of mechanical contact is defined at Z = 0 for all the maps, and all of them are obtained using soft cantilevers.

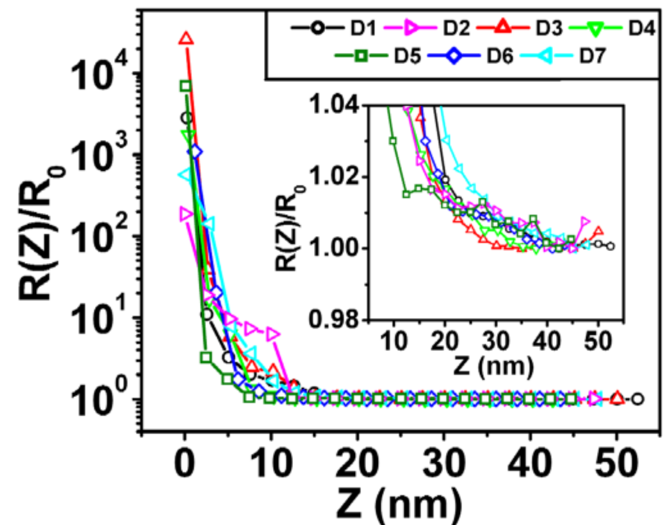

FIG. 7. (Color online) Normalized total resistance $R(Z)/R_0$ vs loading Z for CNTs D1-D7. The zero of the Z-axis indicates the onset of mechanical contact for all curves. The conditions under which each curve is recorded are listed in Table II. The inset shows a detailed view of the load-independent region. All of the curves are averages over three consecutive loading cycles, except for the D4 curve, which is averaged over two cycles only.

We now explore $\Delta R_c(\mathrm{Z})$, which contains useful information about the electro-mechanical formation of the contact between the tip and the CNT. Figure 7 shows $R(\mathrm{Z})/R_0 = (\Delta R_c(\mathrm{Z})/R_0 + 1)$, where $R_0 = R_{nt}(L) + R_{Au} + (R_c)_{\min}$, for current-loading curves of Type-I, taken on the seven CNTs we studied. In these curves, a trend of fast decay can be observed which flattens beyond some characteristic displacement ($\mathrm{Z_c} \approx 15$ nm) into an almost constant level equal to one. This distance can be seen to be largely independent of the CNT type, diameter, and force constant of the cantilever used, given the diversity of parameters under which the data of Fig. 7 are taken, as can be seen from Table II. To understand this result, we first remark that this rather large value of $\mathrm{Z_c}$ excludes tunneling through a constant barrier as the mechanism responsible for this modulation of the contact resistance with load, and attempts to interpret the Z-dependence of the contact resistance as due to tunneling[1] result in unrealistically low (~2 meV) values of the barrier height.

TABLE II. Channel length, load-independent resistance, drain voltage, gate voltage, and type of cantilever used for the data of Fig. 7.

CNT	L (μm)	R_0 (MΩ)	V_d (V)	V_g (V)	Cantilever
D1	26	0.786	0.1	−3	Soft
D2	21.5	0.172	0.1	0	Soft
D3	73	1.2	0.5	−5	Soft
D4	38.9[a]	0.165	0.1	0	Hard
D5	128.8	6.0	0.1	0	Soft
D6	63.4[a]	0.26	0.1	0	Hard
D7	7.3	0.166	0.1	−3	Soft

[a]Disregarding the presence of the loop. The loop junction was poorly conductive at the corresponding gate voltage.

Downloaded 01 Sep 2011 to 129.2.99.26. Redistribution subject to AIP license or copyright; see http://jap.aip.org/about/rights_and_permissions

Instead, we interpret the Z-dependence of the contact resistance as due to the modulation of the barrier for carrier injection from the tip into the CNT by the stress at the contact. This stress-induced modulation of the injection barrier could be associated with deformation of the gold film at the tip, with some stress needed to bring a certain number of gold grains into contact with the CNT.[22] Also, some theoretical calculations predict the presence of a tunnel barrier in the case of gold contacts to CNTs,[23,24] and a dependence of this barrier on the electrode-CNT separation within atomic-scale distances,[24,25] where this tunnel barrier becomes smaller with a smaller metal-CNT distance, which establishes a possible route for the modulation of the contact resistance through contact stress.

We now discuss whether radial deformation of the CNT induced by the tip at the contact point could have played a role in our measurements. The similar behavior of contacts to both metallic and semiconducting CNTs exhibited in all our measurements, and the independence of bias conditions discussed in Sec. III B, seem to contradict some theoretical expectations[10–14] which predict that semiconducting and metallic CNTs respond in a different way to radial deformation, which could open a gap in metallic CNTs, while narrowing the gap for semiconducting CNTs.

The previous attempts to understand this problem[1,8,9] have employed a Hertz contact model between a sphere representing the tip and a cylinder representing the CNT, where the contact force between the tip and the substrate is assumed to be entirely transmitted across the CNT. We believe this picture is unrealistic mainly because it ignores the yielding mechanics of the metallic coating covering the tip. It also ignores the parasitic planar motion of the tip as it contacts the surface previously discussed, and the inevitable presence of asymmetries in cantilever manufacturing and mounting, or microscopic roughness of the tip or substrate. All of these factors can cause some part of the tip to be in touch with the substrate at the contact point, thus invalidating the assumption that force is transmitted from the tip to the substrate entirely across the CNT, which possibly leads to an overestimation of the mechanical stress at the tip-CNT contact.

In particular, an AFM cantilever coated with a ductile metal such as gold would acquire a rather flat profile upon contacting the surface, which suggests that the average stress around the CNT is mainly determined by the mechanics of the substrate/tip contact. In this case, the maximum stress that could be applied by the tip corresponds to the limit of a fully plastic contact, and would be limited to about 2.2 σ_Y, where σ_Y is the yield strength of the coating metal.[26] For gold, σ_Y can have a rather wide range, 55–220 MPa, depending on preparation conditions and sample dimensions.[27] Even by considering the upper limit of these values for σ_Y, the stress around the CNT would still be limited to about 480 MPa. This stress level is significantly lower than the theoretically expected minimum stress required for radial deformation to occur,[28] estimated to be about 700 MPa for a CNT having a diameter around 2 nm,[28] which is approximately the case for all the CNTs we studied, except for D4 and D6. Therefore, radial deformation of these CNTs by a soft metal such as gold is unlikely. In other words, the more rigid CNT is more likely to cut through the more ductile gold and not vice versa. The larger diameter CNTs, D4 and D6 (whose diameters ≈4 nm), were probably multiwalled, and therefore the minimum pressure to cause radial deformation in these is probably higher than the value of ∼100 MPa predicted by Hasegawa *et al*.[28] for a single walled carbon CNT having that diameter.

The assumption that radial stress on the CNT is limited through plastic deformation of the gold coating can also explain the similar values of the characteristic displacement for obtaining a load-independent contact ($Z_c \approx 15$ nm) between soft and hard cantilevers, which apply nominally different forces at the same displacement due to their different spring constants. It is also consistent with our observation of a large disparity in the tip diameters of soft and hard cantilevers, which can be seen in the width of the plateau region through measurements such as Figs. 3(a), 3(b), and 4(b), and was further confirmed through SEM imaging of the tips after these contact experiments were performed. We consistently observe much larger tip diameters for hard cantilevers, suggesting that the larger force for hard cantilevers at a given displacement is spread out over a larger tip area due to plasticity of the gold coating.

D. Temporal stability of the contact

Temporal stability of the contact is an important operational aspect for performing local transport measurements, where the contact needs to be stable for at least the duration of a typical voltage sweep. The contact becomes destabilized through the tip sliding off the CNT, which can happen directly through drift in the X- and Y-directions. Drift in the Z-direction does not directly alter the contact in the load-independent regime. However, it still can indirectly destabilize the contact through parasitic planar motion. Typically, we found the drift to be about 0.2 nm/min for the X and Y directions, and about 0.2 nm/s for the Z direction under warm up conditions, and dropping to less than half these values under steady state conditions. In order to further characterize the temporal stability of our system, we first tuned the lateral position, such as to obtain a current-loading curve of Type-I, and then simultaneously recorded the deflection of the cantilever and the current through the CNT device as a function of time. This was done in two modes, where in the first mode we applied feedback such that the deflection is kept constant, and in the second mode the deflection was left to freely drift. We found that in our system, the current was generally stable within a margin of $\pm 4\%$, for times of 2–6 min in the first (deflection stabilized) mode, and 1–2 min without deflection stabilization. The current fluctuations generally had a $1/f^{\gamma}$ spectrum where $\gamma \approx 1$–1.5, and did not correlate with the deflection fluctuations, which in the frequency range studied (< 50 Hz), showed mostly a white spectrum. These observations suggest that the sources of current fluctuations in the load-independent regime are the $1/f$ and telegraph noise in the CNT channel[29–31] rather than fluctuations of the contact resistance between the CNT and the movable electrode.

Downloaded 01 Sep 2011 to 129.2.99.26. Redistribution subject to AIP license or copyright; see http://jap.aip.org/about/rights_and_permissions

IV. CONCLUSION

It is possible to establish a good and reproducible electrical contact between a conductive AFM cantilever and a CNT. For an optimized placement of the tip relative to the CNT, the contact resistance is independent of the loading force beyond a certain limit, and this behavior is also independent of the bias conditions, and thus is equivalent to a temporary fixed electrode. Under certain conditions of tip placement relative to the CNT, the current through the contact shows non-monotonic behavior with loading. This behavior results largely from the parasitic planar motion of the cantilever during loading. We do not observe any clear evidence indicating a change in the electronic properties of the CNTs caused by loading at the contact point, and suggest that radial stress is largely limited by the plastic deformation of the soft coating metal. The contact is stable in time to within our ability to measure, set by the current fluctuations imposed by $1/f$ and telegraph noise in the CNT channel.

ACKNOWLEDGMENTS

This work has been supported by the University of Maryland NSF-MRSEC under Grant No. DMR 05-20471. MRSEC Shared Experimental Facilities were used in this work.

[1] P. J. de Pablo, M. T. Martínez, J. Colchero, J. Gómez-Herrero, W. K. Maser, A. M. Benito, E. Muñoz, and A. M. Baró, Adv. Mater. **12**, 573 (2000).
[2] P. J. de Pablo, C. Gómez-Navarro, J. Colchero, P. A. Serena, J. Gómez-Herrero, and A. M. Baró, Phys. Rev. Lett. **88**, 036804 (2002).
[3] Y. Yaish, J. Y. Park, S. Rosenblatt, V. Sazonova, M. Brink, and P. L. McEuen, Phys. Rev. Lett. **92**, 046401 (2004).
[4] J. Y. Park, S. Rosenblatt, Y. Yaish, V. Sazonova, H. Ustunel, S. Braig, T. A. Arias, P. W. Brouwer, and P. L. McEuen, Nano Lett. **4**, 517 (2004).
[5] C. Gomez-Navarro, P. J. D. Pablo, J. Gomez-Herrero, B. Biel, F. J. Garcia-Vidal, A. Rubio, and F. Flores, Nature Mater. **4**, 534 (2005).
[6] P. Sundqvist, F. J. Garcia-Vidal, F. Flores, M. Moreno-Moreno, C. Gomez-Navarro, J. S. Bunch, and J. Gomez-Herrero, Nano Lett. **7**, 2568 (2007).
[7] X. Zhou, J.-Y. Park, S. Huang, J. Liu, and P. L. McEuen, Phys. Rev. Lett. **95**, 146805 (2005).
[8] C. Gómez-Navarro, P. J de Pablo, and J. Gómez-Herrero, Adv. Mater. **16**, 549 (2004).
[9] C. Gomez-Navarro, J. J. Saenz, and J. Gomez-Herrero, Phys. Rev. Lett. **96**, 076803 (2006).
[10] C.-J. Park, Y.-H. Kim, and K. J. Chang, Phys. Rev. B **60**, 10656 (1999).
[11] C. Kilic, S. Ciraci, O. Gülseren, and T. Yildirim, Phys. Rev. B **62**, R16345 (2000).
[12] O. Gülseren, T. Yildirim, S. Ciraci, and C. Kilic, Phys. Rev. B **65**, 155410 (2002).
[13] Y. Umeno, T. Kitamura, and A. Kushima, Comput. Mater. Sci. **30**, 283 (2004).
[14] H. Mehrez, A. Svizhenko, M. P. Anantram, M. Elstner, and T. Frauenheim, Phys. Rev. B **71**, 155421 (2005).
[15] Y. Li, W. Kim, Y. Zhang, M. Rolandi, D. Wang, and H. Dai, J. Phys. Chem. B **105**, 11424 (2001).
[16] W. Kim, H. C. Choi, M. Shim, Y. Li, D. Wang, and H. Dai, Nano Lett. **2**, 703 (2002).
[17] S. Heinze, J. Tersoff, R. Martel, V. Derycke, J. Appenzeller, and P. Avouris, Phys. Rev. Lett. **89**, 106801 (2002).
[18] A. Javey, J. Guo, Q. Wang, M. Lundstrom, and H. Dai, Nature (London) **424**, 654 (2003).
[19] J. H. Hoh and A. Engel, Langmuir **9**, 3310 (1993).
[20] L. Huang, C. Meyer, and C. Prater, J. Phys.: Conf. Ser. **61**, 805 (2007).
[21] R. J. Cannara, M. J. Brukman, and R. W. Carpick, Rev. Sci. Instrum. **76**, 053706 (2005).
[22] S.-H. Ke, W. Yang, and H. U. Baranger, J. Chem. Phys. **124**, 181102 (2006).
[23] S. Dag, O. Gulseren, S. Ciraci, and T. Yildirim, Appl. Phys. Lett. **83**, 3180 (2003).
[24] B. Shan and K. Cho, Phys. Rev. B **70**, 233405 (2004).
[25] I. Deretzis and A. L. Magna, Nanotechnology **17**, 5063 (2006).
[26] J. Jamari and D. J. Schipper, J. Tribol. **128**, 230 (2006).
[27] H. D. Espinosa, B. C. Prorok, and B. Peng, J. Mech. Phys. Solids **52**, 667 (2004).
[28] M. Hasegawa and K. Nishidate, Phys. Rev. B **74**, 115401 (2006).
[29] P. G. Collins, M. S. Fuhrer, and A. Zettl, Appl. Phys. Lett. **76**, 894 (2000).
[30] F. Liu, K. L. Wang, C. Li, and C. Zhou, IEEE Trans. Nanotechnol. **5**, 441 (2006).
[31] M. Ishigami, J. H. Chen, E. D. Williams, D. Tobias, Y. F. Chen, and M. S. Fuhrer, Appl. Phys. Lett. **88**, 203116 (2006).

Downloaded 01 Sep 2011 to 129.2.99.26. Redistribution subject to AIP license or copyright; see http://jap.aip.org/about/rights_and_permissions